RSC Advances

PAPER

View Article Online
View Journal | View Issue

Cite this: *RSC Adv.*, 2018, **8**, 31348

A facile route to magnetic mesoporous core–shell structured silicas containing covalently bound cyclodextrins for the removal of the antibiotic doxycycline from water†

Ying Zhang,[a] Fuquan Jiang,[b] Danya Huang,[a] Shushan Hou,[a] Hongli Wang,[a] Minggang Wang,[a] Yue Chi*[a] and Zhankui Zhao*[a]

Received 9th July 2018
Accepted 22nd August 2018

DOI: 10.1039/c8ra05781h

rsc.li/rsc-advances

The excessive use of antibiotics has led to various environmental problems; the control and separation of these antibiotics are important in environmental science. Herein, a novel mesoporous nanocomposite, Fe_3O_4@SiO_2@mSiO_2-CD, has been synthesized for the removal of antibiotic compounds from aqueous media. The well-designed nanocomposite is composed of β-cyclodextrin functionalized surfaces, ordered mesoporous silica shells with large radially oriented mesopores, and nonporous silica-coated magnetic cores (Fe_3O_4). The synergistic action of both the mesoporous structure and the accessible cavity of β-cyclodextrin ensures the good adsorption of doxycycline. Furthermore, the Fe_3O_4@SiO_2@mSiO_2-CD nanocomposite can be collected, separated and easily recycled from aqueous solution using an external magnet.

1. Introduction

Antibiotics are an emerging and important type of environmental contamination, and their removal from aqueous solution has attracted significant research interest due to their potential for causing antibiotic-resistant genes that can result in superbugs.[1–3] Many methods have been applied in the removal of antibiotics from wastewater, such as chlorination,[4] advanced oxidation technology,[5] biodegradation,[6] adsorption and membrane processes.[7] Among these methods, adsorption has received the most attention due to the advantages of easy operation, low cost, high efficiency, and no risk of highly toxic byproducts. Some novel adsorbents include biochar,[8] coconut palm,[9] imprinted materials,[10] natural soils,[11–13] and metal oxides.[14]

Due to the high surface area, large pore volume, regular and tunable pore size, and interconnected frameworks, extensive studies have been focused on using mesoporous silicas for the removal of inorganic pollutants such as heavy metal ions[15–17] and organic hazardous pollutants such as antibiotics, dyes, *etc.*[18–28] However, due to the special nature of antibiotics, unmodified mesoporous silicas exhibit limited ability in their adsorption; therefore, in order to get enhanced adsorption performance, functional groups need to be introduced to alter the surface properties of mesoporous silicas.[29] Currently, there are few efficient modified methods aimed toward the adsorption of antibiotics. Cyclodextrins (CDs) are a class of macrocyclic molecules with a hydrophilic exterior and a lipophilic interior cavity,[30,31] and they can form inclusion complexes with organic molecules that can be trapped in the hydrophobic cavity through host–guest interactions. CDs are also highly water-soluble and thus need to be grafted onto a solid phase such as polymers and porous silicas.

The separation of mesoporous silica adsorbents from the final system is notoriously difficult, even causing secondary pollution. Magnetic separation provides a very convenient method for removing and recycling particles/composites by applying external magnetic fields, and so magnetic nanomaterials are widely used in environmental treatment. Nano Fe_3O_4, a kind of magnetic nanomaterial, has obtained considerable attention due to its high specific surface area and unique superparamagnetism.[32–34] To get enhanced adsorption performance, the preparation of magnetic mesoporous silicas by combining the advantages of mesoporous structure and magnetic properties together could lead to high specific surface area and the ability for magnetic recovery and result in a major leap forward for treating wastewater.

On the basis of comprehensive considerations, we prepared magnetic mesoporous core–shell structured silicas with radially oriented large mesopores and β-cyclodextrin functionalized surfaces, which combine the advantages of the mesoporous

[a]*College of Material Science and Engineering, Key Laboratory of Advanced Structural Materials, Ministry of Education, Changchun University of Technology, Changchun, 130012, China. E-mail: yuechi@ccut.edu.cn; zhaozk@ccut.edu.cn; Fax: +86 431 85716644; Tel: +86 431 85716644*

[b]*China-Japan Union Hospital, Jilin University, Changchun, 130012, China*

† Electronic supplementary information (ESI) available. See DOI: 10.1039/c8ra05781h

structure, suitable surface properties, and good magnetic separability.[35] The β-cyclodextrin functionalized mesoporous silica can be used as a highly efficient adsorbent for trapping doxycycline (DOX), exhibiting high adsorption capacity and immobilization efficiency, and good recycling stability.

2. Experimental

2.1. Chemicals

All chemicals were used as received without any further purification. Ferric chloride ($FeCl_3 \cdot 6H_2O$), tetraethyl orthosilicate (TEOS, 98%), ethylene glycol, ammonia solution (28%), triethanolamine (TEA), cetyltrimethyl ammonium bromide (CTAB), (3-aminopropyl) trimethoxysilane (APTMS), and monochlorotriazinyl β-cyclodextrin (MCT-β-CD) were purchased from Aladdin reagent (Shanghai) Co. Ltd. Doxycycline hydrochloride was purchased from Sinopharm Chemical Reagent Co. Ltd.

2.2. Preparation of Fe_3O_4@SiO_2@mSiO_2-CD microsphere

The core–shell structured mesoporous Fe_3O_4@SiO_2@mSiO_2 microspheres were prepared through a multistep approach according to the published procedure (for details, see ESI†).[36] To introduce covalently bound cyclodextrins, 100 mg MCT-β-CD and 50 mg APTMS were dissolved in 10 mL of deionized water, then 50 mg sodium bicarbonate was added. The solution was magnetically stirred at 40 °C for 30 min, forming a clear solution. After adding 10 mL of ethanol, the white flocculated precipitate of β-cyclodextrin-silica derivative was formed immediately. At this point, 90 mL of deionized water was added under stirring to redissolve the β-cyclodextrin-silica derivative, and then 100 mg of Fe_3O_4@SiO_2@mSiO_2 microspheres were dispersed in the above solution under stirring at room temperature for 24 h. The product was collected with the help of a magnetic field, washed several times with deionized water, and dried at 60 °C for 6 h to obtain Fe_3O_4@SiO_2@mSiO_2-CD microspheres.

2.3. Adsorption experiments

The adsorption isotherms of the DOX on Fe_3O_4@SiO_2@mSiO_2-CD were measured according to the following procedure. Typically, 10 mg Fe_3O_4@SiO_2@mSiO_2-CD was stirred with 20 mL of DOX aqueous solution with a predetermined concentration, and shaken continuously at 298 K for 24 h to ensure adsorption equilibrium. The adsorption kinetics for DOX adsorption on Fe_3O_4@SiO_2@mSiO_2-CD was analyzed by mixing Fe_3O_4@SiO_2@mSiO_2-CD with 20 mL DOX solution (100 mg L^{-1}) at 298 K. At various time intervals, parts of the mixture were separated and the concentration of pollutant remaining in solution was measured. In the adsorption equilibrium and kinetic experiments, the initial pH of the DOX solution was 3.8.

To evaluate the effect of pH, 10 mg of Fe_3O_4@SiO_2@mSiO_2-CD was added to 20 mL of DOX solution with the concentration of 100 mg L^{-1}. The pH of the mixed solution was adjusted using hydrochloric acid or sodium hydroxide in the range of 3 to 11. The mixed solution was constantly stirred for 24 h at 298 K.

To evaluate the effect of temperature, 10 mg Fe_3O_4@SiO_2@mSiO_2-CD was added to 20 mL of DOX solution with predetermined concentrations (10–100 mg L^{-1}). The mixed solution was constantly stirred for 24 h at 298 K or 303 K; the initial pH of the solution, before it was adjusted, was 3.8.

To evaluate the effect of ionic strength, different amounts of NaCl or $CaCl_2$ were added to the DOX solution. The concentration of NaCl or $CaCl_2$ was in the range from 0 to 0.5 mol L^{-1}. Other adsorption procedures were the same as those in the above-mentioned pH-effect experiments.

To study the regeneration ability of Fe_3O_4@SiO_2@mSiO_2-CD, 10 mg of Fe_3O_4@SiO_2@mSiO_2-CD was added to 20 mL of DOX solution with the concentration of 100 mg L^{-1}. Since methanol has a strong polarity, it is often used as the detergent for mineral surface organic substances and can effectively remove organic matter and thus reproduce the adsorbent. Fe_3O_4@SiO_2@mSiO_2-CD loaded with DOX was therefore treated with a methanol solution (60%, v/v) under ultrasonication for 1 h. The product was collected with the help of a magnet field, followed by repeated washing with deionized water and ethanol. Finally, the product was vacuum dried at 50 °C. We repeated the above procedure for four cycles.

2.4. Characterizations

The morphologies of the as-prepared nanocomposite were observed using scanning electron microscopy (SEM, JEOL JSM-5600), energy dispersive X-ray (EDX), and transmission electron microscopy (TEM, JEM-2000). The surface chemical properties of the samples were determined using Fourier transform infrared spectroscopy (FT-IR, Bio-Rad, FTS 6000). The nitrogen adsorption and desorption isotherms were measured at 77 K on a Micromeritics ASAP 2020 plus HD88 instrument (Micromeritics Instrument Corp, Norcross, GA). The Brunauer–Emmett–Teller (BET) specific surface area was calculated using desorption data. The pore size distribution curves were calculated from the analysis of the desorption branch of the isotherm using the Barrett–Joyner–Halenda algorithm. X-ray diffraction (XRD) patterns were collected using a Bruker D8 Advance X-ray diffractometer to identify the crystal and channel structure with a Cu Kα X-ray source operating at 9 kV and 200 mA for small-angle X-ray scanning. UV-visible absorption spectra were recorded using a UV-visible spectrophotometer (Cary-5000) to monitor the absorption process.

3. Results and discussions

3.1. Cyclodextrin-modified magnetic mesoporous nanomaterials

The mesoporous organic–inorganic hybrid silica Fe_3O_4@SiO_2@mSiO_2-CD can be fabricated through a multistep approach (Scheme 1). As shown in Scheme 1, Fe_3O_4@SiO_2@mSiO_2 microspheres were prepared using solvothermal reaction, the Stöber method and surfactant templating approach. The corresponding TEM and SEM images of samples at each step are presented in Fig. S1.† Fe_3O_4, Fe_3O_4@SiO_2 and Fe_3O_4@SiO_2@mSiO_2 microspheres exhibited a nearly spherical

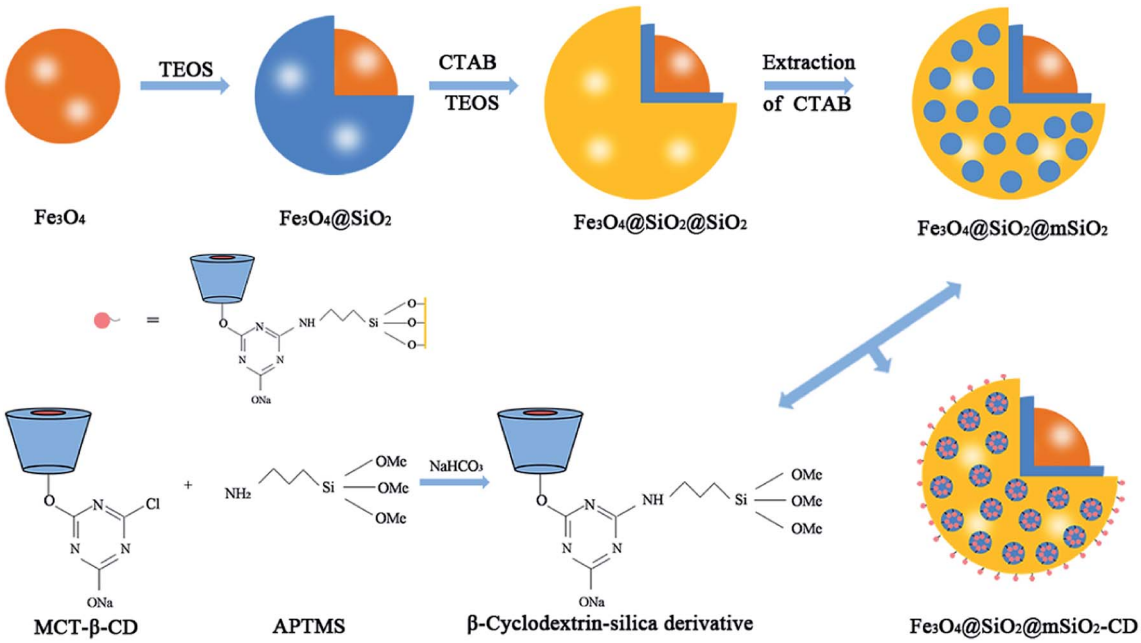

Scheme 1 Schematic illustration of the formation of Fe_3O_4@SiO_2@mSiO_2-CD microspheres.

shape with a mean diameter of about 350 nm, 420 nm and 510 nm, respectively. The Fe_3O_4@SiO_2@mSiO_2 microspheres were nearly monodisperse with a clearly distinguishable three-layer structure including a Fe_3O_4 core, a SiO_2 interlayer, and a mesoporous SiO_2 outer layer with large radially oriented mesopores. In order to produce an efficient adsorbent for antibiotics, we developed a facile method to activate Fe_3O_4@SiO_2@mSiO_2, resulting in β-cyclodextrin functionalized Fe_3O_4@SiO_2@mSiO_2-CD. As illustrated in Scheme 1, β-cyclodextrin was introduced into the pore channels through a grafting approach, and the APTMS as a linker that reacted with MCT-β-CD forming the β-cyclodextrin-silica derivative was attached to the pore channels. Therefore, the Fe_3O_4@SiO_2@mSiO_2-CD microspheres have β-cyclodextrin and triazinyl groups that can provide multiple interactions, including inclusion interactions, hydrophobic interactions, electrostatic attractions, and π–π interactions, to achieve an efficient adsorbent for antibiotics. It can be seen that the Fe_3O_4@SiO_2@mSiO_2-CD microspheres are still a clearly three-layer structure with diameter of about 510 nm. As shown in Fig. 1, the Fe_3O_4@SiO_2@mSiO_2-CD microspheres still retain the morphological properties of Fe_3O_4@SiO_2@mSiO_2, which were well dispersed without the occurrence of aggregation and the radially oriented large mesopores were well preserved after surface modification. The wide-angle XRD pattern of Fe_3O_4@SiO_2@mSiO_2-CD exhibited almost the same features as pure Fe_3O_4, except for a broad peak centered at 22° of 2θ (Fig. S2†), indicating that the coated SiO_2 is amorphous.[37] The EDX characterization demonstrates that Fe_3O_4@SiO_2@mSiO_2-CD contains necessary and diagnostic elements (Fe, Si, O, C and N), indicating the presence of functional groups (Fig. S3†).

Fig. 2 shows the FTIR spectra of Fe_3O_4@SiO_2@mSiO_2 and Fe_3O_4@SiO_2@mSiO_2-CD. As can be seen, Fe_3O_4@SiO_2@mSiO_2 shows framework bands at 1081 cm^{-1} and 799 cm^{-1}, attributed to the anti-symmetric stretching and symmetric stretching frequencies of Si–O–Si,[37,38] respectively. The broad peak at 3416 cm^{-1} is attributed to the O–H stretching vibrations, indicating the presence of surface hydroxyl groups and

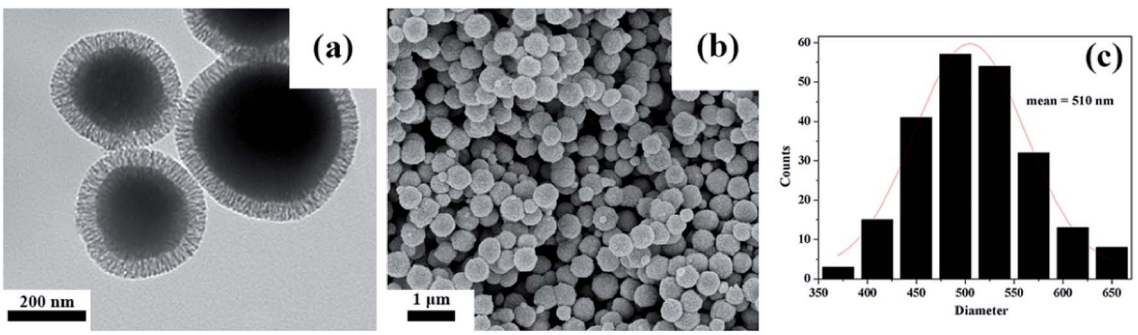

Fig. 1 TEM and SEM of Fe_3O_4@SiO_2@mSiO_2-CD (a and b), and the size distribution histogram of Fe_3O_4@SiO_2@mSiO_2-CD microspheres calculated from SEM images (c).

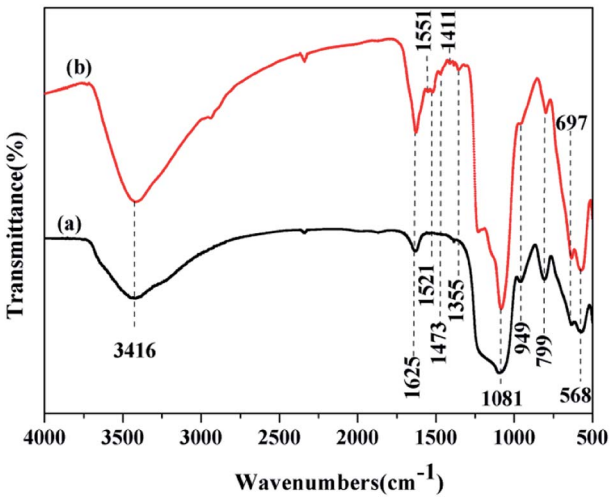

Fig. 2 FTIR spectra of Fe_3O_4@SiO_2@mSiO_2 (a), and Fe_3O_4@SiO_2@mSiO_2-CD (b).

chemisorbed water.[39] The bands observed at 568 cm^{-1} and 963 cm^{-1} were characteristic of Fe–O stretching vibrations and stretching modes of surface Si–OH, respectively. In addition to the peaks that correspond to Fe_3O_4@SiO_2@mSiO_2, the FTIR spectrum of Fe_3O_4@SiO_2@mSiO_2-CD exhibits the vibration peaks around 1625–1400 cm^{-1} assigned to triazinyl groups and the peak at 2938 cm^{-1} assigned to C–H stretching of methyl groups, which suggest that the β-cyclodextrin was successfully introduced upon grafting.

N_2 adsorption–desorption isotherms of the Fe_3O_4@SiO_2@mSiO_2 and Fe_3O_4@SiO_2@mSiO_2-CD show type IV curves with H1 hysteresis loops (Fig. 3A), indicating uniform mesopores. From the pore size distribution curves (Fig. 3B), the samples exhibit similar pore size distribution in the range of 5–25 nm. Compared with Fe_3O_4@SiO_2@mSiO_2, the pore size, surface area and pore volumes of Fe_3O_4@SiO_2@mSiO_2-CD were reduced (Table 1), which can be attributed to the introduction of functional groups in the mesopores according to previous studies.[40] However Fe_3O_4@SiO_2@mSiO_2-CD can still exhibit the large specific surface area and pore size, suggesting that the surface modification method in this work is suitable and the highly open mesopores can be preserved. The small angle XRD patterns of Fe_3O_4@SiO_2@mSiO_2 and Fe_3O_4@SiO_2@mSiO_2-CD microspheres show an obvious diffraction peak between $2\theta = 2°$ and 3°, indicating an ordered mesostructure (Fig. 3C). After surface modification, a decrease in the intensities and a slight shifting of the peaks to higher angles were observed, suggesting that the functional groups were grafted inside the pores.

Magnetization curves of the Fe_3O_4@SiO_2@mSiO_2 and Fe_3O_4@SiO_2@mSiO_2-CD exhibit near-zero coercivity and remanence, suggesting their superparamagnetic nature (Fig. 4). Fe_3O_4@SiO_2@mSiO_2 and Fe_3O_4@SiO_2@mSiO_2-CD nanocomposites have magnetization saturation (M_s) values of 33.59 and 30.99 emu g^{-1}, respectively. Because of the introduction of functional groups, the M_s value of Fe_3O_4@SiO_2@mSiO_2-CD slightly decreased as compared with that of Fe_3O_4@SiO_2@mSiO_2. However, the core–shell structured Fe_3O_4@SiO_2@mSiO_2-CD nanocomposite still showed strong magnetization, indicating its suitability for magnetic separation and recovery. The Fe_3O_4@SiO_2@mSiO_2-CD microspheres can be quickly attracted to the side of the vial with the aid of a magnet, leaving the solution transparent (Fig. 4, inset), and can be well redispersed by shaking the vial.

3.2. Adsorption kinetics and effect of time

As shown in Fig. 5, the adsorption capacity increased rapidly in the initial 6–10 h, and then slowly increased, finally reaching equilibrium. The initial rapid increase can be interpreted as the DOX molecules filling the open and cyclodextrin-functionalized

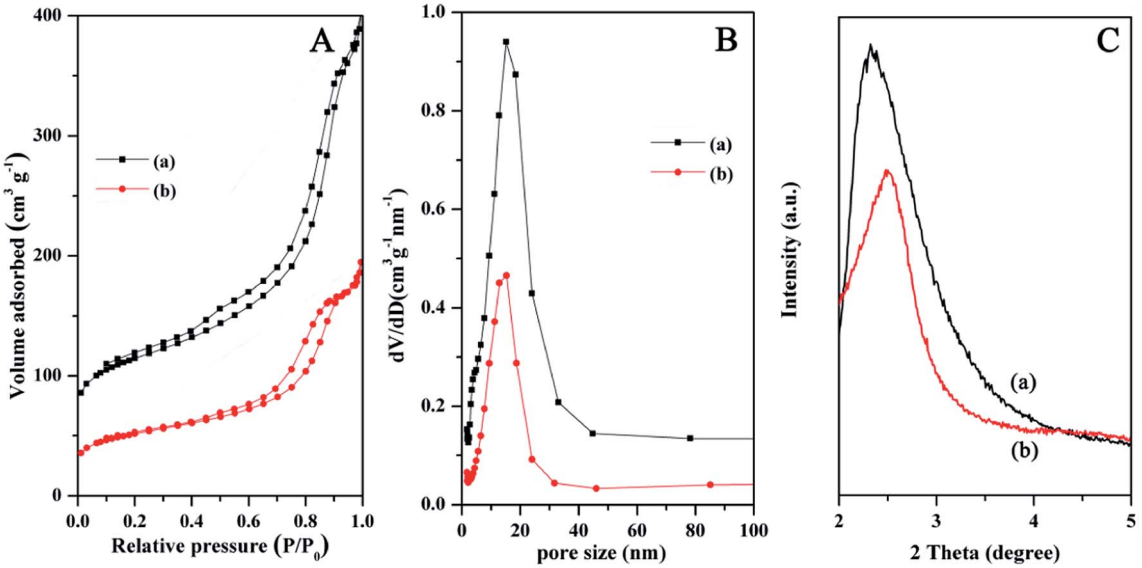

Fig. 3 N_2 adsorption–desorption isotherms (A), the pore size distributions (B), and small-angle XRD patterns (C) of Fe_3O_4@SiO_2@mSiO_2 (a) and Fe_3O_4@SiO_2@mSiO_2-CD (b) microspheres.

Table 1 Textural properties of Fe_3O_4@SiO_2@mSiO_2 and Fe_3O_4@SiO_2@mSiO_2-CD microspheres

Sample	Pore size (nm)	BET surface area ($m^2\ g^{-1}$)	Pore volume ($cm^3\ g^{-1}$)
Fe_3O_4@SiO_2@mSiO_2	9.5	234	0.53
Fe_3O_4@SiO_2@mSiO_2-CD	9.4	119	0.27

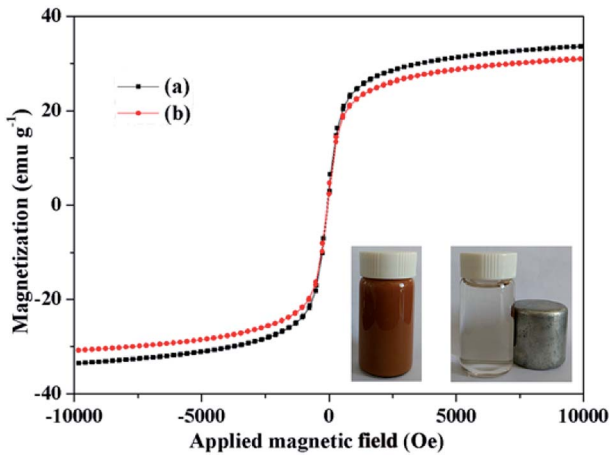

Fig. 4 Magnetization curves of Fe_3O_4@SiO_2@mSiO_2 (a) and Fe_3O_4@SiO_2@mSiO_2-CD (b). The inset is the separation process of the Fe_3O_4@SiO_2@mSiO_2-CD microspheres using a magnet.

mesopores. For wastewater treatment applications, the contact time is an important parameter. A short adsorption equilibrium contact time is beneficial. The contact time required for antibiotics adsorption using Fe_3O_4@SiO_2@mSiO_2-CD adsorbent is very short compared to other reported adsorbents such as activated carbon.

In order to study the DOX adsorption kinetics, several kinetic models were used to fit the experimental data. The pseudo-first order kinetic model and the pseudo-second-order equation[41–48] are often used to represent the kinetic adsorption of antibiotics onto the adsorbents, which can be represented in eqn S1.† The

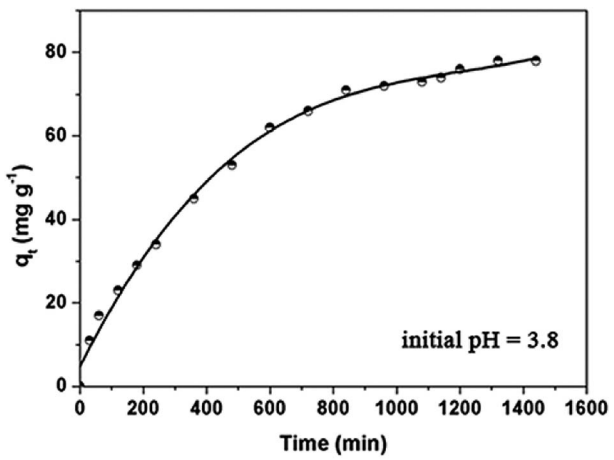

Fig. 5 Adsorption kinetics of DOX onto the Fe_3O_4@SiO_2@mSiO_2-CD adsorbents at 298 K. Initial concentration = 100 mg L^{-1}.

Table 2 Kinetic model parameters for the adsorption of DOX onto the Fe_3O_4@SiO_2@mSiO_2-CD

Pseudo-first-order			Pseudo-second-order		
K_1 (min^{-1})	q_e (mg g^{-1})	R^2	K_2 (g mg^{-1} h^{-1})	q_e (mg g^{-1})	R^2
0.002	443	0.986	0.008	83.33	0.984

DOX adsorption onto Fe_3O_4@SiO_2@mSiO_2-CD microspheres is a complicated process that not only involves physical diffusion and adsorption but also possibly involves chemical bonding and reactions. The applied kinetic models provided parameters and the regression coefficients, R^2, as shown in Table 2. It can be seen for the DOX adsorption onto Fe_3O_4@SiO_2@mSiO_2-CD that the pseudo-second-order R^2 (0.984) is slightly lower than R^2 (0.986) of the pseudo-first-order model. However, according to the pseudo-second-order model, the calculated maximum adsorption capacity (83.33 mg g^{-1}) is close to the actual experimental data (78 mg g^{-1}), suggesting that DOX adsorption onto the Fe_3O_4@SiO_2@mSiO_2-CD corresponds to the pseudo-second-order model to a greater extent. This result indicated that the adsorption process was due to chemisorption. However, considering the reasonably good fit to the pseudo-first-order model as well, we propose that both chemisorption and physisorption might take place in this adsorption system.

3.3. Adsorption isotherm

Adsorption isotherms can help to understand the interactions between the adsorbent and the adsorbate in the adsorption process. Fig. 6 shows the adsorption isotherms for DOX adsorbed onto the prepared adsorbent Fe_3O_4@SiO_2@mSiO_2-CD microspheres at 298 K. It can be observed that the amount of DOX adsorbed gradually increases with the concentration of DOX. Fe_3O_4@SiO_2@mSiO_2 and Fe_3O_4@SiO_2@mSiO_2-CD maximum adsorption capacity can reach 34 mg g^{-1} and 78 mg g^{-1}, respectively. This means that the presence of functional groups on the surface of the adsorbent enhanced the adsorption of DOX.

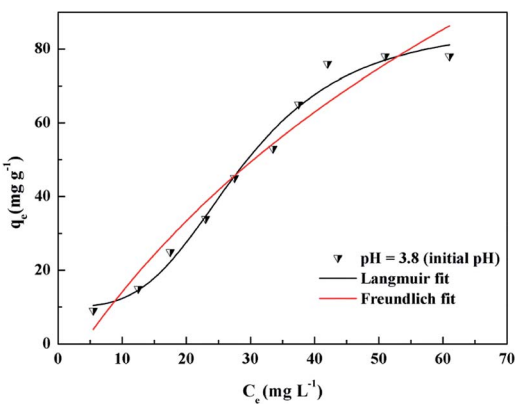

Fig. 6 Adsorption isotherms of DOX onto the Fe_3O_4@SiO_2@mSiO_2-CD adsorbents.

Table 3 Langmuir, Freundlich and D–R isotherm parameters for the adsorption of DOX onto Fe_3O_4@SiO_2@mSiO_2-CD adsorbents (298 K)

Langmuir			Freundlich			D–R		
K_L (L mg^{-1})	q_m (mg g^{-1})	R^2	K_F (mg g^{-1})	$1/n$	R^2	q_m (mg g^{-1})	E (kJ mol^{-1})	R^2
0.134	200	0.984	2.683	0.987	0.981	45.70	7.45	0.785

To further understand the adsorption mechanism of DOX onto the Fe_3O_4@SiO_2@mSiO_2-CD materials, the Langmuir, Freundlich and Dubinin–Radushkevich (D–R) adsorption models[49] were used to fit the experimental data (Fig. 6). The Langmuir, Freundlich, and D–R isotherm models are presented in eqn S2.† The Langmuir model assumes the adsorption of a single layer covering the surface, *i.e.*, uniform adsorption. The Freundlich equation can be applied to non-ideal sorption on heterogeneous surfaces as well as multi-layer sorption. The adsorption model parameters are listed in Table 3. The Langmuir isotherm model gave a higher correlation coefficient (R^2 = 0.984) for the DOX adsorption on the adsorbent than the Freundlich isotherm (R^2 = 0.981), indicating the monolayer coverage of DOX onto the adsorbent. This result indicates that the adsorption process fits the Langmuir model to a greater extent as compared to the Freundlich model. Furthermore, under the initial pH conditions, the Langmuir separation factor K_L was between 0 and 1. It could be inferred that the adsorption process was quite favorable at the studied concentrations used in this study.[50] The D–R isotherm model describes the adsorption process from the energy perspective and can provide the sorption energy E, and can then indicate whether the adsorption process is physical adsorption or chemical adsorption.[51–53] For the initial pH, the value of E was 7.45 kJ mol^{-1}, suggesting that the adsorption process might be dominated by the physical mechanism.[54,55] The weak physical forces, such as the hydrophobic effect, electrostatic attractions and hydrogen bonding might affect DOX adsorption onto Fe_3O_4@SiO_2@mSiO_2-CD. However, because of the low value of R^2 (0.785) in this study, and from E, it may be deduced that this physisorption hypothesis has limitations.

3.4. Effect of pH on DOX adsorption on Fe_3O_4@SiO_2@mSiO_2-CD

The pH of the DOX solution significantly affects the adsorption process, so the appropriate pH value can improve the adsorption efficiency and adsorption capacity. In order to explore the effects of the pH on the removal of DOX, HCl or NaOH solutions were used to adjust the pH of the DOX solution in the range of 3–11. Fig. 7 shows the DOX structural formula.

As shown in Fig. 8A, for pH < 8.0, the adsorption capacity increased with the pH, while for pH > 8.0, it decreased. DOX molecules have tricarbonylamide, phenolic diketone and dimethylamine groups, so depending on the solution pH, DOX can exist as cationic (pH < 3.27), zwitterionic (3.27 < pH < 7.32), neutral, and anionic forms (pH > 7.32).[56] For pH < 3.27, in the aqueous solution, the cationic form is the dominant species and the electrostatic interactions with the DOX molecules and the adsorbent are weak; therefore, the quantity of DOX adsorbed onto Fe_3O_4@SiO_2@mSiO_2-CD is suppressed. As the pH increased from 3.27, the interaction between DOX and sorbent increased, mainly because of a decrease in the cationic concentration and the increase in the zwitterionic concentration; *i.e.*, the zwitterionic form is dominant. When the pH was 8.0, the maximum adsorption of DOX was obtained, mainly because the Fe_3O_4@SiO_2@mSiO_2-CD surface cyclodextrin structure provided hydrophobic sites that can interact with the DOX molecules *via* the hydrophobic effect. As the concentration of ions increased at higher pH, a progressive decrease in the adsorption was observed, which could be attributed to the increased negative charge of the Fe_3O_4@SiO_2@mSiO_2-CD surface, the decreased electrostatic attraction between the Fe_3O_4@SiO_2@mSiO_2-CD and the negatively charged DOX. Based on the experimental data (Fig. 8A), the adsorption capacity of DOX significantly changed when the pH increased, indicating that electrostatic interactions have a major effect in the adsorption process. However, the adsorption capacity showed little change in the pH range of 5.0 to 6.0 and 10.0 to 11.0. This indicates that besides the electrostatic interaction effect, the cyclodextrin cavity also had a hydrophobic effect in the adsorption process.

3.5. Effect of temperature and adsorption thermodynamics

The effect of temperature on DOX adsorption was investigated at 298 K and 303 K under different initial concentrations. As shown in Fig. 8B, the amounts adsorbed onto the Fe_3O_4@SiO_2@mSiO_2-CD were reduced when the temperature increased. The reason may be that hydrogen bonds form between DOX molecules and the surface of the

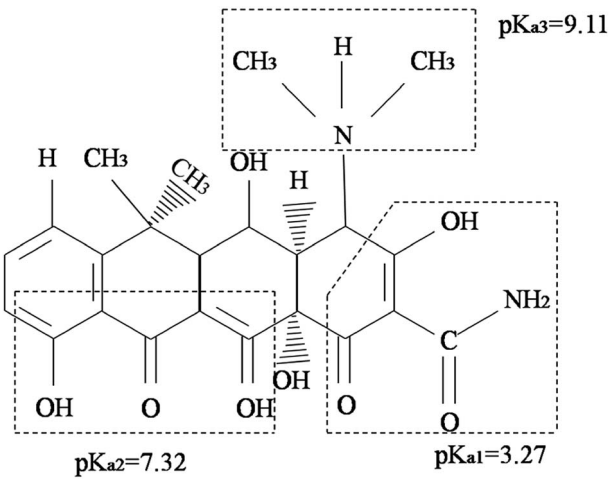

Fig. 7 Molecular structure and ionization constants of DOX.

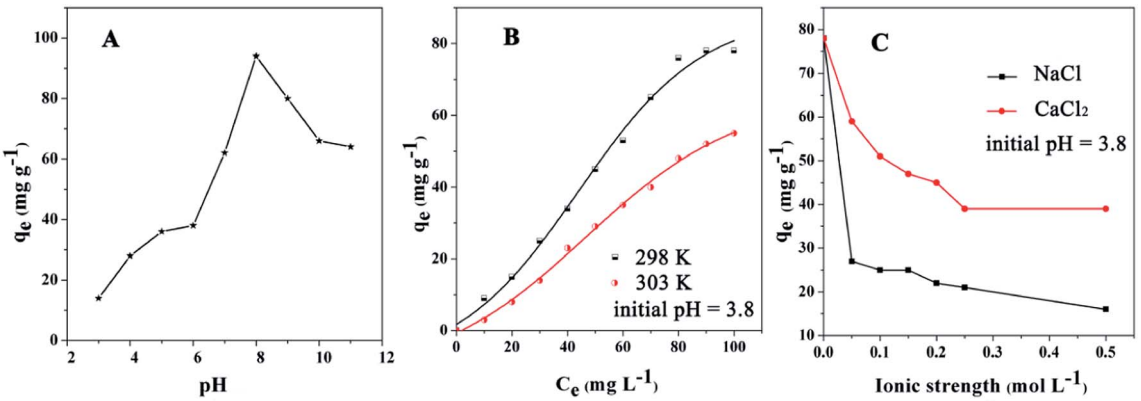

Fig. 8 The effects of (A) pH, (B) temperature, and (C) ionic strength on Fe_3O_4@SiO_2@mSiO_2-CD for the adsorption of DOX antibiotics (initial concentration = 100 mg L^{-1}).

Fe_3O_4@SiO_2@mSiO_2-CD.[57–59] The DOX molecule possesses one benzene ring, three aromatic heterocyclic groups, and several moieties capable of forming hydrogen bonds with the functional groups on the surface of Fe_3O_4@SiO_2@mSiO_2-CD. Because the hydrogen bond formation releases heat, when the temperature increased, the hydrogen bond effect could lead to a reduction in the adsorbed amount.

To further study the nature of the sorption process, the thermodynamic parameters such as the Gibbs free energy (ΔG^0), the enthalpy (ΔH^0), and the entropy (ΔS^0)[60] were analyzed. The equations are presented in eqn S3,† and the results are presented in Table 4; the negative value of ΔH^0 (−17.31 kJ mol^{-1}) for DOX indicated the exothermic nature of the adsorption process. The exothermic characteristics revealed that the adsorption process was more favorable at lower temperatures, which was consistent with the experimental results. Furthermore, ΔG^0 value was −0.41 kJ mol^{-1} at 298 K, and the negative value of ΔG^0 indicates that the adsorption process was spontaneous and the type of adsorption was physical adsorption.[61] Therefore, in the process of DOX adsorption onto Fe_3O_4@SiO_2@mSiO_2-CD, physical forces did exist. Further, the value of ΔG^0 increased and became positive at 303 K, indicating that the adsorption of DOX by Fe_3O_4@SiO_2@mSiO_2-CD was suppressed at this temperature.

3.6. Effect of ionic strength

The effects of ionic strength (NaCl, $CaCl_2$) on DOX adsorption by the adsorbent are depicted in Fig. 8C for Na^+ and Ca^{2+} concentrations from 0 M to 0.5 M. The effect of ionic strength was relatively strong on the DOX adsorption; the amounts of DOX adsorbed by Fe_3O_4@SiO_2@mSiO_2-CD decreased with increasing ionic concentration. Fe_3O_4@SiO_2@mSiO_2-CD has accommodative hydrophobic cavities, where interactions with DOX can occur. Theoretically, in the salting-out effect, when the Na^+ and Ca^{2+} are added, the solubility of DOX in water decreases and so a larger amount of DOX will be adsorbed on the surface of the adsorbent; however, the practical result is the opposite.[62] DOX molecules contain –NH_2 and –OH electron-donor groups, which can form stable complexes with Na^+ and Ca^{2+}.[63] Since the metal complexes improve DOX solubility in water, the amount of adsorbed DOX on Fe_3O_4@SiO_2@mSiO_2-CD decreases. DOX molecules contain C=O and O–H groups, which might form hydrogen bonds with the functional groups on the surface of the Fe_3O_4@SiO_2@mSiO_2-CD.[64] However, the metal complexes would restrict the hydrogen bond formation, resulting in lower adsorbed DOX amounts. Further, this restriction of the hydrogen bonds formation becomes stronger with increasing Na^+ and Ca^{2+} concentrations.

Table 4 Thermodynamic parameters for DOX adsorption onto Fe_3O_4@SiO_2@mSiO_2-CD

Temperature (K)	K_c (L g^{-1})	ΔG^0 (kJ mol^{-1})	ΔS^0 (kJ mol^{-1} K^{-1})	ΔH^0 (kJ mol^{-1})
298	1.42	−0.41	−0.02	−17.31
303	0.49	2.21		

3.7. Regenerability of the adsorbents

The recycling and regeneration of the adsorbent are important in practical applications. As shown in Fig. 9, the adsorption

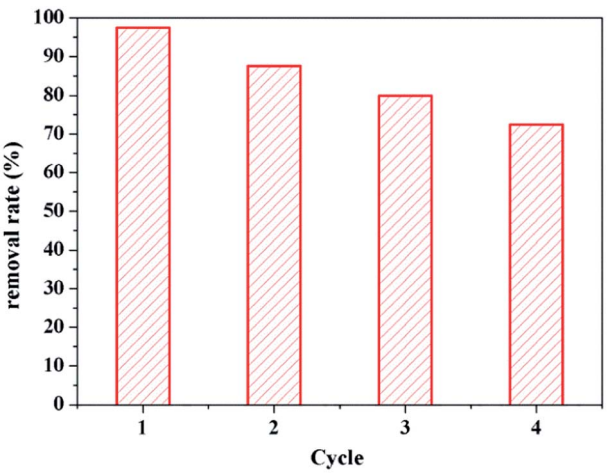

Fig. 9 Sorption–desorption cycles of Fe_3O_4@SiO_2@mSiO_2-CD microspheres.

efficiency decreased slightly in sequential cycles, but the reusability was over 80% even after four cycles, suggesting that the unique textural structure and surface properties of Fe_3O_4@SiO_2@mSiO_2-CD result in stability and reusability.

4. Conclusions

In this work, we designed and developed a magnetic responsive mesoporous core–shell structured material, Fe_3O_4@SiO_2@mSiO_2-CD, with covalently bound cyclodextrins and radially oriented large mesopores. The synergistic action of both mesoporous structure and accessible cavity of β-cyclodextrin ensures the good adsorption of DOX. Hydrophobic effects, hydrogen bonds, and electrostatic interactions play important roles in DOX adsorption onto Fe_3O_4@SiO_2@mSiO_2-CD. The adsorption kinetics of the adsorbent follow the pseudo-second-order model and the adsorption isotherm data fit well with the Langmuir model. The thermodynamic parameters derived from the results show that the adsorption process of DOX is spontaneous and exothermic. In addition, the adsorbent can be easily removed from aqueous solution by magnetic separation and is easily regenerated; therefore, this material is promising for the removal of antibiotics from wastewater.

Conflicts of interest

There are no conflicts to declare.

Acknowledgements

This work was supported by the National Natural Science Foundation of China (Grant no. 51608050, 51601018 and 51671035), and the Science and Technology Research Project of the Education Department of Jilin Province (Grant no. 2016327).

References

1 D. Hughes and D. I. Andersson, Environmental and genetic modulation of the phenotypic expression of antibiotic resistance, *FEMS Microbiol. Rev.*, 2017, **41**(3), 374–391.
2 B. Kasprzyk-Hordern, R. M. Dinsdale and A. J. Guwy, The removal of pharmaceuticals, personal care products, endocrine disruptors and illicit drugs during wastewater treatment and its impact on the quality of receiving waters, *Water Res.*, 2009, **43**(2), 363–380.
3 G. Dantas, M. O. A. Sommer, R. D. Oluwasegun, *et al.*, Bacteria Subsisting on Antibiotics, *Science*, 2008, **320**(5872), 100–103.
4 W. Ben, Y. Shi, W. Li, *et al.*, Oxidation of sulfonamide antibiotics by chlorine dioxide in water: Kinetics and reaction pathways, *Chem. Eng. J.*, 2017, **327**, 743–750.
5 I. Michaelkordatou, P. Karaolia and D. Fattakassinos, The role of operating parameters and oxidative damage mechanisms of advanced chemical oxidation processes in the combat against antibiotic-resistant bacteria and resistance genes present in urban wastewater, *Water Res.*, 2018, **129**, 208.
6 D. A. Alexandrino, A. P. Mucha, C. M. Almeida, *et al.*, Biodegradation of the veterinary antibiotics enrofloxacin and ceftiofur and associated microbial community dynamics, *Sci. Total Environ.*, 2017, **581**, 359–368.
7 V. Sharma, R. V. Kumar, K. Pakshirajan, *et al.*, Integrated adsorption-membrane filtration process for antibiotic removal from aqueous solution, *Powder Technol.*, 2017, **321**, 259–269.
8 W. Gwenzi, N. Chaukura, C. Noubactep, *et al.*, Biochar-based water treatment systems as a potential low-cost and sustainable technology for clean water provision, *J. Environ. Manage.*, 2017, **197**, 732–749.
9 F. P. Camacho, V. S. Sousa, R. Bergamasco, *et al.*, The use of Moringa oleifera, as a natural coagulant in surface water treatment, *Chem. Eng. J.*, 2016, **226–237**, 226–237.
10 M. Razali, J. F. Kim, M. Attfield, *et al.*, Sustainable wastewater treatment and recycle in membrane manufacturing, *Green Chem.*, 2015, **17**(12), 5196–5205.
11 R. A. Figueroa and A. A. Mackay, Sorption of Oxytetracycline to Iron Oxides and Iron Oxide-Rich Soils, *Environ. Sci. Technol.*, 2005, **39**(17), 6664–6671.
12 J. Mon, M. Flury and J. B. Harsh, Sorption of four triarylmethane dyes in a sandy soil determined by batch and column experiments, *Geoderma*, 2006, **133**(3), 217–224.
13 S. Wang and H. Wang, Adsorption behavior of antibiotic in soil environment:a critical review, *Front. Environ. Sci. Eng.*, 2015, **9**(4), 565–574.
14 T. D. Pham, T. T. Do, V. L. Ha, *et al.*, Adsorptive removal of ammonium ion from aqueous solution using surfactant-modified alumina, *Environ. Chem.*, 2017, **14**(5), 327–337.
15 J. Ma, K. Jia, G. Cheng, *et al.*, Solid-Phase Extraction of Pb(II) Ions Based on L-Cysteine Functionalized Fe_3O_4/SiO_2 Core-Shell Nanoparticles, *J. Environ. Eng.*, 2016, **142**(11), 04016062.
16 Y. Huang, C. Yang, Z. Sun, *et al.*, Removal of cadmium and lead from aqueous solutions using nitrilotriacetic acid anhydride modified ligno-cellulosic material, *RSC Adv.*, 2015, **5**(15), 11475–11484.
17 H. J. He, Z. H. Xiang, X. J. Chen, *et al.*, Biosorption of Cd(II) from synthetic wastewater using dry biofilms from biotrickling filters, *Int. J. Environ. Sci. Technol.*, 2018, **15**(7), 1491–1500.
18 A. C. Pradhan and K. M. Parida, Facile synthesis of mesoporous composite Fe/Al_2O_3-MCM-41: An efficient adsorbent/catalyst for swift removal of methylene blue and mixed dyes, *J. Mater. Chem.*, 2012, **22**(15), 7567–7579.
19 A. Walcarius, M. Etienne and B. Lebeau, Rate of Access to the Binding Sites in Organically Modified Silicates. 2. Ordered Mesoporous Silicas Grafted with Amine or Thiol Groups, *Chem. Mater.*, 2003, **15**(11), 2161–2173.
20 V. Antochshuk and M. Jaroniec, 1-Allyl-3-propylthiourea modified mesoporous silica for mercury removal, *Chem. Commun.*, 2002, (3), 258.
21 W. Huang, Y. Zhu, J. Tang, *et al.*, Lanthanum-doped ordered mesoporous hollow silica spheres as novel adsorbents for efficient phosphate removal, *J. Mater. Chem. A*, 2014, **2**(23), 8839–8848.

22 W. Huang, Y. Zhu, J. Tang, *et al.*, Lanthanum-doped ordered mesoporous hollow silica spheres as novel adsorbents for efficient phosphate removal, *J. Mater. Chem. A*, 2014, **2**(23), 8839–8848.

23 M. V. Lombardo, M. Videla, A. Calvo, *et al.*, Aminopropyl-modified mesoporous silica SBA-15 as recovery agents of Cu(II)-sulfate solutions: Adsorption efficiency, functional stability and reusability aspects, *J. Hazard. Mater.*, 2012, **223–224**(2), 53–62.

24 E. Da'Na and A. Sayari, Adsorption of heavy metals on amine-functionalized SBA-15 prepared by co-condensation: Applications to real water samples, *Desalination*, 2012, **285**(1), 62–67.

25 J. Aguado, J. M. Arsuaga and A. Arencibia, Influence of synthesis conditions on mercury adsorption capacity of propylthiol functionalized SBA-15 obtained by co-condensation, *Microporous Mesoporous Mater.*, 2008, **109**(1–3), 513–524.

26 M. Mureseanu, A. Reiss, N. Cioatera, *et al.*, Mesoporous silica functionalized with 1-furoyl thiourea urea for Hg(II) adsorption from aqueous media, *J. Hazard. Mater.*, 2010, **182**(1–3), 197–203.

27 L. Zhang, W. Zhang, J. Shi, *et al.*, A new thioether functionalized organic-inorganic mesoporous composite as a highly selective and capacious Hg^{2+} adsorbent, *Chem. Commun.*, 2003, (2), 210–211.

28 K. Li, Z. Zeng, J. Xiong, *et al.*, Fabrication of mesoporous Fe_3O_4@SiO_2@CTAB–SiO_2, magnetic microspheres with a core/shell structure and their efficient adsorption performance for the removal of trace PFOS from water, *Colloids Surf., A*, 2015, **465**, 113–123.

29 J. Fujiki, H. Yamada and K. Yogo, Enhanced adsorption of carbon dioxide on surface-modified mesoporous silica-supported tetraethylenepentamine: Role of surface chemical structure, *Microporous Mesoporous Mater.*, 2015, **215**, 76–83.

30 F. Hirayama and K. Uekama, Cyclodextrin-based controlled drug release system, *Adv. Drug Delivery Rev.*, 1999, **36**(1), 125–141.

31 M. Lahiani-Skiba, Y. Boulet, I. Youm, *et al.*, Interaction between hydrophilic drug and α-cyclodextrins: physico-chemical aspects, *J. Inclusion Phenom. Macrocyclic Chem.*, 2007, **57**(1–4), 211–217.

32 S. H. Wu, H. J. He, X. Li, C. P. Yang, G. M. Zeng, B. Wu, S. Y. He and L. Lu, Insights into atrazine degradation by persulfate activation using composite of nanoscale zero-valent iron and graphene: Performances and mechanisms, *Chem. Eng. J.*, 2018, **341**, 126–136.

33 J. Yu, H. He, W. L. Yang, *et al.*, Magnetic bionanoparticles of Penicillium, sp. yz11-22N_2 doped with Fe_3O_4, and encapsulated within PVA-SA gel beads for atrazine removal, *Bioresour. Technol.*, 2018, **260**, 196–203.

34 C. y. Zhu, H. J. He, C. P. Yang, *et al.*, Preparation, performances and mechanisms of magnetic Saccharomyces cerevisiae bionanocomposites for atrazine removal, *Chemosphere*, 2018, **200**, 380–387.

35 J. H. Wen, H. P. Shang, H. J. Choi, *et al.*, Core–shell structured mesoporous magnetic nanoparticles and their magnetorheological response, *Colloids Surf., A*, 2017, **524**, 79–86.

36 H. Yuhshan, Citation review of Lagergren kinetic rate equation on adsorption reactions, *Scientometrics*, 2004, **59**(1), 171–177.

37 T. D. Pham, C. M. Vu and H. J. Choi, Enhanced fracture toughness and mechanical properties of epoxy resin with rice husk-based nano-silica, *Polym. Sci.*, 2017, 1–8.

38 C. Kannan, T. Sundaram and T. Palvannan, Environmentally stable adsorbent of tetrahedral silica and non-tetrahedral alumina for removal and recovery of malachite green dye from aqueous solution, *J. Hazard. Mater.*, 2008, **157**(1), 137–145.

39 S. F. Motevalizadeh, M. Khoobi, A. Sadighi, *et al.*, Lipase immobilization onto polyethylenimine coated magnetic nanoparticles assisted by divalent metal chelated ions, *J. Mol. Catal. B: Enzym.*, 2015, **120**, 75–83.

40 Y. Feng, Y. Liu, L. Xue, *et al.*, Carboxylic acid functionalized sesame straw: A sustainable cost-effective bioadsorbent with superior dye adsorption capacity, *Bioresour. Technol.*, 2017, **238**, 675–683.

41 Y. Liu and Y. J. Liu, Biosorption isotherms, kinetics and thermodynamics, *Sep. Purif. Technol.*, 2008, **61**(3), 229–242.

42 H. Xu, J. H. Tay, S. K. Foo, *et al.*, Removal of dissolved copper(II) and zinc(II) by aerobic granular sludge, *Water Sci. Technol.*, 2004, **50**(9), 155.

43 J. C. Y. Ng, Kinetics of pollutant sorption by biosorbents: review, *Sep. Purif. Rev.*, 2000, **29**(2), 189–232.

44 M. Erdem and A. Ozverdi, Kinetics and thermodynamics of Cd(II) adsorption onto pyrite and synthetic iron sulphide, *Sep. Purif. Technol.*, 2006, **51**(3), 240–246.

45 I. Kiran, T. Akar, A. S. Ozcan, *et al.*, Biosorption kinetics and isotherm studies of Acid Red 57 by dried *Cephalosporium aphidicola*, cells from aqueous solutions, *Biochem. Eng. J.*, 2006, **31**(3), 197–203.

46 E. Rubin, P. Rodriguez, R. Herrero, *et al.*, Removal of Methylene Blue from aqueous solutions using as biosorbent *Sargassum muticum*: an invasive macroalga in Europe, *J. Chem. Technol. Biotechnol., Biotechnol.*, 2010, **80**(3), 291–298.

47 S. W. Won, H. J. Kim, S. H. Choi, *et al.*, Performance, kinetics and equilibrium in biosorption of anionic dye Reactive Black 5 by the waste biomass of Corynebacterium glutamicum, as a low-cost biosorbent, *Chem. Eng. J.*, 2006, **121**(1), 37–43.

48 K. V. Kumar, S. Sivanesan and V. Ramamurthi, Adsorption of Malachite Green onto Pithophora sp. a Fresh Water Algae: Equilibrium and Kinetic Modelling, *Process Biochem.*, 2005, **40**(8), 2865–2872.

49 H. Sharififard, F. Pepe, P. Aprea, *et al.*, Chemical modification of activated carbon surface with iron functional groups for efficient separation of vanadium: batch and column study, *Res. Chem. Intermed.*, 2017, (1), 1–18.

50 Y. S. Ho, Comment on equilibrium and kinetics studies of adsorption of copper(II) on chitosan and chitosan/PVA beads, *Int. J. Biol. Macromol.*, 2006, **38**(2), 148.
51 K. Vijayaraghavan, T. V. Padmesh, K. Palanivelu, *et al.*, Biosorption of nickel(II) ions onto *Sargassum wightii*: application of two-parameter and three-parameter isotherm models, *J. Hazard. Mater.*, 2006, **133**(1), 304–308.
52 M. L. Jackson, Ion exchangers in analytical chemistry, *Agron. J.*, 1953, **45**(12), 654–655.
53 S. Tunali, T. Akar, A. S. Özcan, *et al.*, Equilibrium and kinetics of biosorption of lead(II) from aqueous solutions by *Cephalosporium aphidicola*, *Sep. Purif. Technol.*, 2006, **47**(3), 105–112.
54 L. Zhang, X. Song, X. Liu, *et al.*, Studies on the removal of tetracycline by multi-walled carbon nanotubes, *Chem. Eng. J.*, 2011, **178**(24), 26–33.
55 M. J. Ahmed and S. K. Theydan, Microwave assisted preparation of microporous activated carbon from Siris, seed pods for adsorption of metronidazole antibiotic, *Chem. Eng. J.*, 2013, **214**, 310–318.
56 S. A. Sassman and L. S. Lee, Sorption of three tetracyclines by several soils: assessing the role of pH and cation exchange, *Environ. Sci. Technol.*, 2005, **39**(19), 7452–7459.
57 K. Yang and B. Xing, ChemInform Abstract: Adsorption of Organic Compounds by Carbon Nanomaterials in Aqueous Phase: Polanyi Theory and Its Application, *Chem. Rev.*, 2010, **110**(10), 5989–6008.
58 P. Oleszczuk, B. Pan and B. S. Xing, Adsorption and desorption of oxytetracycline and carbamazepine by multiwalled carbon nanotubes, *Environ. Sci. Technol.*, 2010, **44**(12), 9167–9173.
59 L. Ji, W. Chen, S. Zheng, *et al.*, Adsorption of Sulfonamide Antibiotics to Multiwalled Carbon Nanotubes, *Langmuir*, 2009, **25**(19), 11608.
60 X. Zhu, Y. Liu, F. Qian, *et al.*, Preparation of magnetic porous carbon from waste hydrochar by simultaneous activation and magnetization for tetracycline removal, *Bioresour. Technol.*, 2014, **154**(2), 209–214.
61 Z. Bekçi, Y. Seki and M. K. Yurdakoç, A study of equilibrium and FTIR, SEM/EDS analysis of trimethoprim adsorption onto K10, *J. Mol. Struct.*, 2007, **827**(1), 67–74.
62 T. D. Pham, M. Kobayashi and Y. Adachi, Adsorption of Polyanion onto Large Alpha Alumina Beads with Variably Charged Surface, *Adv. Phys. Chem.*, 2014, **2014**, 9.
63 M. E. Parolo, M. J. Avena, G. R. Pettinari, *et al.*, Influence of Ca^{2+} on tetracycline adsorption on montmorillonite, *J. Colloid Interface Sci.*, 2012, **368**(1), 420–426.
64 M. Seredych and T. J. Bandosz, Adsorption of ammonia on graphite oxide/aluminium polycation and graphite oxide/zirconium-aluminium polyoxycation composites, *J. Colloid Interface Sci.*, 2008, **324**(1), 25–35.